Combustion, Explosion, and Shock Waves, Vol. 46, No. 1, pp. 103–110, 2010

Detonation-Driven Fracture in Thin Shell Structures: Numerical Studies

Ch. Gato[1] and Yinling Shie[1]

UDC 539.3

Translated from *Fizika Goreniya i Vzryva*, Vol. 46, No. 1, pp. 117–125, January–February, 2010.
Original article submitted July 21, 2008; revision submitted April 1, 2009.

Combustion that follows a gas explosion quickly evolves into detonation and causes severe damage in thin-walled structures, especially structures that contain small internal flaws. Detonation-driven fracture of thin structures is studied numerically by a 3D meshfree method. Such scenarios are studied through numerical analysis and compared to experimental data.

Key words: fracture, detonation, combustion, explosion, shell, numerical analysis.

INTRODUCTION

Detonation-driven fracture of thin-walled structures plays an important role in pipe and vessel technology [1–5]. Especially critical are such failures when delicate fluids are stored in such structures. Numerical analysis is often used to predict reliability of such thin-walled structures [6]. However, a coupled numerical analysis involving gas explosion, fracture of the thin-walled structure, and interaction between the structure and the gas is highly complicated and, to the best knowledge of the authors, has not been successfully conducted so far. Large deformations and complicated contact algorithms hamper the development of reliable numerical techniques. One numerical technique that is promising for such types of applications is the meshfree methods [7–13]. The meshfree methods commonly exploit the Lagrangian formulation [14–21] for both the fluid and structure elements, but do not suffer drawbacks of Lagrangian-based finite-element methods. They can handle large deformation and also fracture in a natural manner. We will use a meshfree method to model detonation-driven fracture of thin-walled structures.

The numerical simulation of thin shell structures has been a challenge in applied mechanics and in many engineering branches for many years. There are three major approaches. One is based on the shell theory, another one on the degenerated continuum theory, and the last one is the direct three-dimensional continuum approach. The first two approaches result in complicated numerical methods, which are difficult to implement, especially for complicated phenomena involving interaction with fluids. Therefore, we chose the direct three-dimensional continuum approach. The major drawback of this approach is that it is often required to deploy multiple meshfree nodes in the thin shell thickness direction to acquire reasonable gradient fields, which, on the other hand, leads to degrading the conditioning of the discrete system and then the accuracy of the numerical solution. Moreover, the direct continuum approach is very expensive, which usually requires more elements in the same simulation than the shell theory approach or the degenerated approach does.

Most meshfree methods proposed so far have focused on a continuum-based approach. A meshfree thin shell formulation based on the Kirchhoff–Love theory and on the element-free Galerkin (EFG) method [7] has been developed by Krysl and Belytschko [22] in the context of the small-strain linear elastic framework. Rabczuk et al. [23] extended this work with the consideration of a non-linear elastic material under finite strains and focused on fracture. In the following work, Rabczuk and Areias [24] have simplified the treatment of cracks in a thin shell by using an extrinsic basis. Donning and Liu [25] noted the advantage of meshfree approximations in addressing shear locking in the Mindlin type of beams and plates and have developed a meshfree formulation based on the reproducing kernel particle method (RKPM) [8]. This methodology has

[1]Harbin Engineering University, College of Mechanical Engineering, Harbin, P. R. China; yshie@ymail.com.

been further extended by Kanok-Nukulchai et al. [26] with the use of the EFG method. The EFG method has been employed by Noguchi et al. [27] for shell and membrane structures, in which bi-cubic and quartic basis functions have been introduced to avoid shear and membrane locking. Wang and Chen [28] showed that the Kirchhoff mode in the Mindlin plate can be reproduced using EFG or RKPM if the second-order polynomial basis is used in the moving least-squares approximation. By implementing this with a nodal integration and stabilization scheme, they have shown that the formulation is stable and free of shear locking. Yagawa and Miyamura [29] have developed a free mesh method in which the discrete Kirchhoff theory is combined with the mixed approach. In the case of three-dimensional continuum models, Li et al. [30] have presented a formulation based on RKPM and have studied nonlinear large deformation of thin shells.

In this paper, we use the three-dimensional continuum approach for both the gas explosion and the thin shell. Since the interaction between the gas and the thin shell is complicated and not incorporated into our program, we first model the gas explosion in a rigid tube. The pressures measured over time of this simulation is applied as the boundary condition to our shell model. Fracture of the shell is modeled by breaking links between particles once a certain fracture criterion is met.

FORMULATION AND MESHFREE METHOD

We use the weak form of the conservation of linear momentum within the total Lagrangian framework. This is equivalent to stating that the weak form of the momentum equation is derived in the initial configuration and is given as

$$\delta W = \delta W_{\text{int}} - \delta W_{\text{ext}} + \delta W_{\text{kin}} = 0, \tag{1}$$

where

$$\delta W_{\text{int}} = \int_{\Omega_0} \nabla_X \delta \boldsymbol{u} : \boldsymbol{P} d\Omega_0,$$

$$\delta W_{\text{ext}} = \int_{\Gamma_{0t}} \delta \boldsymbol{u} \cdot \bar{\boldsymbol{t}}_0 d\Gamma_0 + \int_{\Omega_0} \rho_0 \delta \boldsymbol{u} \cdot \boldsymbol{b} d\Omega_0,$$

$$\delta W_{\text{kin}} = \int_{\Omega_0} \rho_0 \delta \boldsymbol{u} \cdot \ddot{\boldsymbol{u}} d\Omega_0.$$

In these equations, W_{int} and W_{ext} denote the internal and external energy, respectively, W_{kin} denotes the kinetic energy, X are the material coordinates, Ω_0 is the domain in the initial configuration, Γ_0 the boundary in the initial configuration, $\boldsymbol{b}$ denotes the body force, ρ_0 is initial density, $\boldsymbol{u}$ is the displacement, $\boldsymbol{P}$ is the first Piola–Kirchhoff stress tensor, $\bar{\boldsymbol{t}}_0$ is the applied traction, and ∇_X denotes spatial derivatives with respect to material coordinate; superimposed dots denote material time derivatives.

The boundary conditions are

$$\boldsymbol{u} = \bar{\boldsymbol{u}}, \quad \boldsymbol{X} \in \Gamma_{0u},$$

$$\boldsymbol{n}_0 \boldsymbol{P} = \boldsymbol{t}_0 = \bar{\boldsymbol{t}}_0, \quad \boldsymbol{X} \in \Gamma_{0t},$$

and the boundaries are $\Gamma_{0u} \cup \Gamma_{0t} = \Gamma_0$ and $\Gamma_{0u} \cap \Gamma_{0t} = 0$. Hereby, the indices t and u refer to the traction boundaries and displacement boundaries, respectively; $\boldsymbol{n}$ is the normal to the traction boundary.

The meshfree approximation $\boldsymbol{u}^h(\boldsymbol{X})$ of a given function $\boldsymbol{u}(\boldsymbol{X})$ can be expressed as the product of the shape functions with nodal parameters $\boldsymbol{u}_J$ as in the finite-element method with n particles:

$$\boldsymbol{u}^h(\boldsymbol{X}) = \sum_{J=1}^{n} N_J(\boldsymbol{X}) \boldsymbol{u}_J = \boldsymbol{N}\boldsymbol{u}. \tag{2}$$

In the element-free Galerkin meshfree method, the shape functions can be derived from moving least-square approximations [7] as

$$\boldsymbol{N}^T(\boldsymbol{X}) = \boldsymbol{p}^T(\boldsymbol{X}) \boldsymbol{A}^{-1}(\boldsymbol{X}) \boldsymbol{P} \boldsymbol{W}(\boldsymbol{X}),$$

the quantity

$$\boldsymbol{A}(\boldsymbol{X}) = \boldsymbol{P}(\boldsymbol{Y}) W(\boldsymbol{X}) \boldsymbol{P}^T(\boldsymbol{Y})$$

is called the moment matrix, and the matrix $\boldsymbol{P}^T(\boldsymbol{Y})$ contains the polynomial basis $\boldsymbol{p}$ that includes polynomials up to the order of two (i.e., quadratic polynomials). Note that linear polynomial completeness is required for convergence in the Galerkin method. The matrix

$$\boldsymbol{W}(\boldsymbol{X}) = \text{diag}\{W_I(\boldsymbol{X} - \boldsymbol{X}_I, h) V_I\} \quad (I = 1, \ldots, n)$$

contains the so-called kernel functions $W_I(\boldsymbol{X} - \boldsymbol{X}_I, h)$, sometimes also called window functions. These kernel function have compact support, and the support size is determined by the dilation parameter h (e.g., the radius in circular supports). We use the quartic spline function that is commonly used in meshfree methods,

$$W(\boldsymbol{X} - \boldsymbol{X}_I, h) = w(s)$$

$$= \begin{cases} 1 - 6s^2 + 8s^3 - 3s^4, & s \leqslant 1, \\ 0, & s > 1, \end{cases}$$

where $s = (\boldsymbol{X} - \boldsymbol{X}_I)/2h$ for the circular support size. More details of the formulation can be found, for instance, in [7, 8].

The test and trial functions have the structure of Eq. (2). Introducing them into the weak formulation with the Bubnov–Galerkin method yields

$$\sum_{I=1}^{n}\delta\boldsymbol{u}_I\Big\{\sum_{J=1}^{n}\Big(-\int_{\Omega_0}\nabla_X N_I(\boldsymbol{X})\boldsymbol{P}d\Omega_0 + \int_{\Omega_0}N_I(\boldsymbol{X})\boldsymbol{b}d\Omega_0+\int_{\Gamma_{0t}}N_I(\boldsymbol{X})\bar{\boldsymbol{t}}_0 d\Gamma_0 + \int_{\Omega_0}\rho_0 N_I(\boldsymbol{X})N_J(\boldsymbol{X})\boldsymbol{u}d\Omega_0\Big)\Big\}=0.$$

After some algebraic operations, the matrix form of this equation can be derived as

$$\boldsymbol{M}_{IJ}\ddot{\boldsymbol{u}}_J=-\boldsymbol{f}_I^{\text{ext}}+\boldsymbol{f}_I^{\text{int}},$$

where

$$\boldsymbol{M}_{IJ}=\int_{\Omega_0}\rho_0\boldsymbol{N}_I(\boldsymbol{X})\boldsymbol{N}_J^T(\boldsymbol{X})d\Omega_0,$$

$$\boldsymbol{f}_I^{\text{ext}}=\int_{\Gamma_{0t}}\boldsymbol{N}_I^T(\boldsymbol{X})\bar{\boldsymbol{t}}_0 d\Gamma_0+\int_{\Omega_0}\boldsymbol{N}_I^T(\boldsymbol{X})\boldsymbol{b}d\Omega_0,$$

$$\boldsymbol{f}_I^{\text{int}}=\int_{\Omega_0}\nabla_X\boldsymbol{N}_I^T(\boldsymbol{X})\boldsymbol{P}d\Omega_0.$$

CONSTITUTIVE MODEL AND FAILURE CRITERION

We use a thermo-elasto-viscoplastic solid model [31] to evaluate the stress term in Eq. (1). In preliminary studies, we found that thermo-effects play a significant role in failure of the shell. The constitutive model is based on the formulation in the rate form:

$$\tau^{\nabla}=\boldsymbol{C}:(\boldsymbol{D}-\boldsymbol{D}^{vp}-\alpha\dot{T}\boldsymbol{I}).$$

Here, $\boldsymbol{C}$ is the first-order elasticity tensor, $\boldsymbol{D}$ is the symmetric part of the velocity gradient $\boldsymbol{L}$, $\tau^{\nabla}=\dot{\tau}-\boldsymbol{W}\cdot\tau-\tau\cdot\boldsymbol{W}$ is the Jaumann rate of the Kirchhoff stress, where $\boldsymbol{W}$ is the antimetric part of the velocity gradient, α is the thermal expansion coefficient, and $\boldsymbol{I}$ is the second-order identity matrix. The viscoplastic overstress model here is based on the von Mises model

$$\boldsymbol{D}^{vp}=\frac{3\bar{\dot{\varepsilon}}}{2\bar{\sigma}}\tilde{\boldsymbol{s}},$$

where

$$\tilde{\boldsymbol{s}}=\boldsymbol{s}-\boldsymbol{a},\quad \boldsymbol{s}=\tau-1/3tr(\tau)\boldsymbol{I},\quad \bar{\sigma}=3/2\tilde{\boldsymbol{s}}:\tilde{\boldsymbol{s}},$$

and $\boldsymbol{a}$ is the back stress, set to zero in our studies. The thermo-viscoplastic flow is governed by the following power law:

$$\bar{\dot{\varepsilon}}=\dot{\varepsilon}_0\left(\frac{\bar{\sigma}}{g(\bar{\varepsilon},T)}\right)^m,$$

$$g(\bar{\varepsilon},T)=\bar{\sigma}\left(1+\frac{\bar{\varepsilon}}{\varepsilon_0}\right)^n\left(1-\delta\left[\exp\frac{T-T_0}{\varkappa}-1\right]\right).$$

Here, $\dot{\varepsilon}_0$ is the reference strain rate, m is the rate sensitivity parameter, σ_0 is the yield stress, $\varepsilon_0=\sigma_0/E$ is the corresponding reference strain, E is Young's modulus, n is the strain hardening exponent, T_0 is the reference temperature, and δ and $\varkappa$ are the thermal softening parameters. The function $g(\bar{\varepsilon},T)$ is the stress–strain relation measured at a quasi-static strain rate $\dot{\varepsilon}$ at a temperature T. The equivalent plastic strain $\bar{\varepsilon}$ is defined as

$$\bar{\varepsilon}=\int_0^t\bar{\dot{\varepsilon}}dt=\int_0^t\sqrt{\frac{2}{3}\boldsymbol{D}^{vp}:\boldsymbol{D}^{vp}}\,dt.$$

Softening in the material due to temperature is accounted for by varying the material parameters

$$E(T)=E_0-1.6\cdot10^6(T-T_0)-10^5(T-T_0)\ [\text{Pa}],$$
$$\nu=\nu_0+5\cdot10^{-5}(T-T_0),$$
$$\sigma_0(T)=\sigma_0-1.5\cdot10^3(T-T_0)^2\ [\text{Pa}],$$
$$\alpha(T)=[2.2+0.0016(T-T_0)]\cdot10^{-5}\ [\text{K}^{-1}],$$

where ν is Poisson's ratio at a temperature T.

The constitutive update scheme for the thermo-elasto-viscoplastic model is largely based on the tangent modulus approach developed by Peirce [32]. The essence of the rate tangent modulus method is to approximate any function of time in the interval $t_{n+\theta}\in[t_n,t_{n+1}]$ as

$$f_\theta=(1-\theta)f_n+\theta f_{n+1}.$$

Thus, with the predicted velocity field $\boldsymbol{v}_{n+1}^{\text{trial}}\boldsymbol{v}_n+\Delta t\boldsymbol{a}_n$, it follows that

$$\boldsymbol{v}_\theta=(1-\theta)\boldsymbol{v}_n+\theta\boldsymbol{v}_{n+1}^{\text{trial}}=\boldsymbol{v}_n+\theta\Delta t\boldsymbol{a}_n,$$
$$\boldsymbol{u}_\theta=(1-\theta)\boldsymbol{u}_n+\theta\boldsymbol{u}_{n+1}=\boldsymbol{u}_n+\theta\Delta t\boldsymbol{v}_n+\theta^2\Delta t^2\boldsymbol{a}_n,$$
$$\boldsymbol{L}_\theta=\nabla_X\boldsymbol{v}_\theta\cdot\boldsymbol{F}_{n+1}^{-1},$$

where $\boldsymbol{a}_n$ denotes the acceleration at the time n and $\boldsymbol{F}$ is the deformation gradient. With $\theta=0.5$, we again recover a central difference scheme. To update the Kirchhoff stress, we proceed as follows:

$$\tau_{n+1}=\tau_n+\dot{\tau}\Delta t,\qquad(3)$$
$$\dot{\tau}\approx\tau^{\nabla}+\boldsymbol{W}_\theta\cdot\tau_n+\tau_n\cdot\boldsymbol{W}_\theta^T.$$

Certainly, one has to find first $\bar{\dot{\varepsilon}}_\theta$ before τ^{∇}. Let

$$\bar{\dot{\varepsilon}}_\theta=(1-\theta)\bar{\dot{\varepsilon}}_n+\theta\bar{\dot{\varepsilon}}_{n+1},$$

where $\bar{\dot{\varepsilon}}_{n+1}$ is approximated by a first-order Taylor series expansion in $\bar{\sigma}$, $\bar{\varepsilon}$, and T:

$$\bar{\dot{\varepsilon}}_{n+1}=\bar{\dot{\varepsilon}}_n+\Delta t_n\left(\frac{\partial\bar{\dot{\varepsilon}}}{\partial\bar{\sigma}}\bigg|_n\dot{\bar{\sigma}}_\theta+\frac{\partial\bar{\dot{\varepsilon}}}{\partial\bar{\varepsilon}}\bigg|_n\bar{\dot{\varepsilon}}_\theta+\frac{\partial\bar{\dot{\varepsilon}}}{\partial T}\bigg|_n\dot{T}_\theta\right).$$

We assume that the temperature update proceeds first, and $\dot{T}_\theta$ comes in handy. Based on the plastic consistency condition and constitutive relations, one may find that

$$\dot{\bar{\varepsilon}}_\theta \approx \frac{\dot{\bar{\varepsilon}}_n}{1+\zeta_\theta} + \frac{\zeta_\theta}{H_\theta(1+\zeta_\theta)}\left(\boldsymbol{P}_\theta : \boldsymbol{D}_\theta + \dot{T}_\theta\left(\frac{\partial\dot{\bar{\varepsilon}}/\partial T}{\partial\dot{\bar{\varepsilon}}/\partial\bar{\sigma}}\right)_n\right),$$

where

$$\boldsymbol{P}_\theta = \boldsymbol{C} : \boldsymbol{p}_n, \quad \boldsymbol{p}_n = \frac{3\tilde{\boldsymbol{s}}}{2\bar{\sigma}},$$

$$H_\theta \approx \left.\frac{\partial\dot{\bar{\varepsilon}}/\partial\bar{\varepsilon}}{\partial\dot{\bar{\varepsilon}}/\partial\bar{\sigma}}\right|_n + (\boldsymbol{p} : \boldsymbol{L} : \boldsymbol{p})_n,$$

$$\zeta_\theta \approx \theta\Delta t\left(\frac{\partial\dot{\bar{\varepsilon}}}{\partial\bar{\sigma}}\right)_n H_\theta, \quad \frac{\partial\dot{\bar{\varepsilon}}}{\partial\bar{\sigma}} = \frac{m\dot{\bar{\varepsilon}}}{\bar{\sigma}},$$

$$\left.\frac{\partial\dot{\bar{\varepsilon}}/\partial T}{\partial\dot{\bar{\varepsilon}}/\partial\bar{\sigma}}\right|_n = -\left(\frac{\bar{\sigma}}{g(\bar{\varepsilon},T)}\right)\frac{\partial g}{\partial T}.$$

Following the rate tangent modulus approach [32], the objective rate of the Kirchhoff stress can be given as

$$\tau^\nabla = \boldsymbol{C}_\theta^{\tan} : \boldsymbol{D}_\theta - \frac{\dot{\bar{\varepsilon}}_n}{1+\zeta_\theta}\boldsymbol{P}_\theta$$

$$- \frac{\zeta_\theta}{(1+\zeta_\theta)H_\theta}\left.\frac{\partial\dot{\bar{\varepsilon}}/\partial T}{\partial\dot{\bar{\varepsilon}}/\partial\bar{\sigma}}\right|_n \dot{T}_\theta\boldsymbol{P}_\theta - \alpha\dot{T}_\theta\boldsymbol{C} : \boldsymbol{I},$$

where

$$\boldsymbol{C}_\theta^{\tan} = \boldsymbol{C} - \left(\frac{\zeta}{(1+\zeta)H}\right)_\theta \boldsymbol{P}_\theta : \boldsymbol{P}_\theta.$$

Once the objective rate is obtained, the Kirchhoff stress can then be updated according to Eq. (3). The corresponding first Piola–Kirchhoff stress tensor is then given as $\boldsymbol{P} = \boldsymbol{F}^{-1} \cdot \tau$.

Failure is incorporated by a stress-based criterion. If the maximum principal tensile stress thrice exceeds the tensile strength σ_0 of the material, then the links between the neighboring particles are broken. This is a similar approach as in the visibility method [33, 34], but it is computationally more effective. More sophisticated models of failure will be studied in the future.

RESULTS

We numerically study the experiments of detonation-driven fracture of tubes done by Chao [35]. The test-setup consists of a detonation tube 152 cm long to which a thin-walled aluminum tube is attached. The lengths of the aluminum tube range from 45.7 cm to 89.6 cm. The inner tube radius is 1.975 cm, and the shell thickness is 0.89 mm. While the lower end of the device is closed, a thin diaphragm seals up the other end (whereto the tube to be tested is attached). At the longitudinal mid-position, the tube has a notch 1, 2, or 3 inches long. The notch depth is 0.6 mm in all cases. The entire apparatus is filled with a combustible mixture of ethylene and oxygen. The initial pressure varies from 80 to 180 kPa. The mixture is thermally

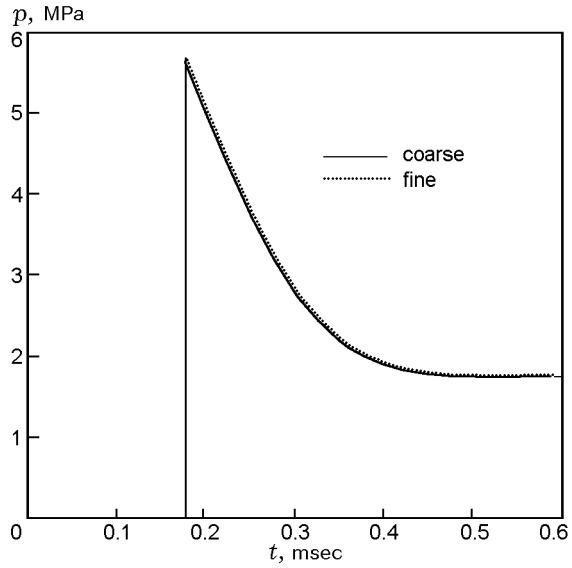

Fig. 1. Pressure over the time for a particle close to the notch from a pure fluid simulation of gas detonation in a rigid tube.

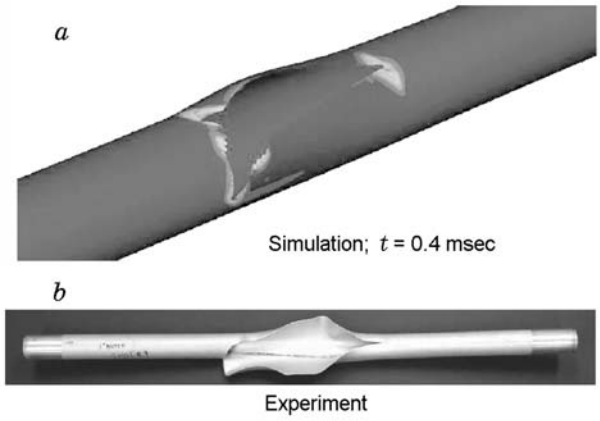

Fig. 2. Displaced configuration and effective stress of the detonation-driven fracture of a cylinder (the notch length is 1 inch).

ignited at the closed end, and the combustion transitions quickly to a detonation. When the detonation wave enters the test specimen, the detonation is close to the Chapman–Jouguet (CJ) limit of quasi-stationary self-sustained propagation. Its velocity is between 2300 and 2400 m/sec, and the pressure values in the fully recreated CJ state range from 2.6 to 6.1 MPa (depending on the initial pressure).

The detonation simulation in the rigid tube is done first. Therefore, we also use the meshfree method.

We consider only the simplified case of a single exothermic chemical reaction $A \rightarrow B$ with a progress variable Y corresponding to the mass fraction ratio be-

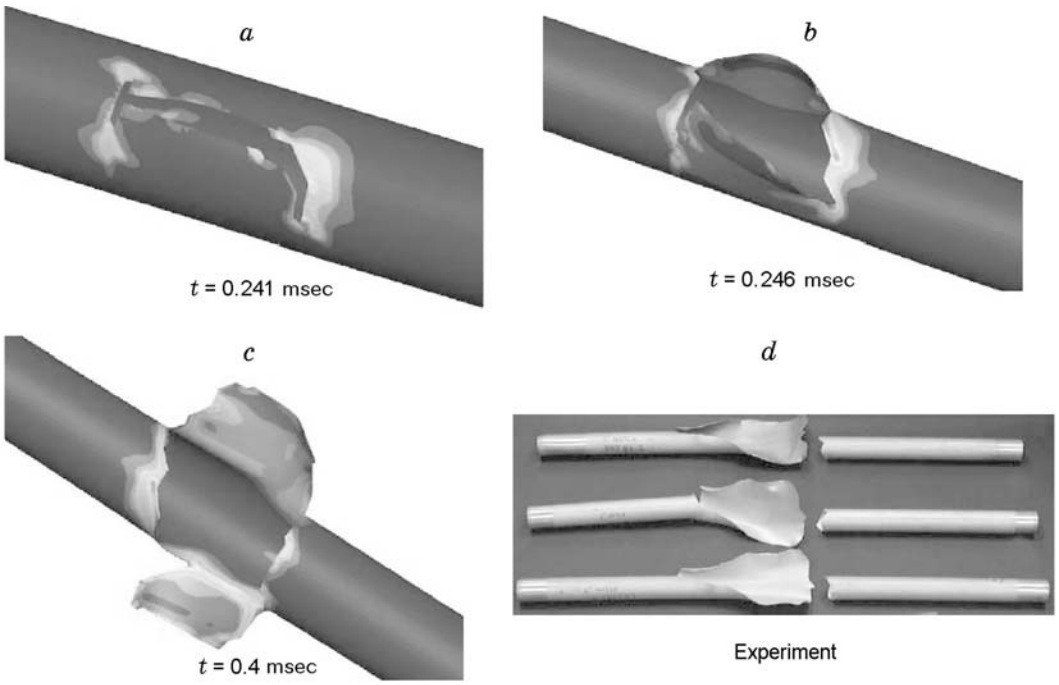

Fig. 3. Displaced configuration and effective stress of the detonation-driven fracture of a cylinder at different times (the notch length is 2 inches): Fig. 3d shows the fracture patterns from three different experiments.

tween the partial density of the reactant A and the total density ρ, i.e., $Y = \rho_A/\rho$. The reaction is incorporated into the Euler equations with the additional inhomogeneous conservation law

$$(\dot{Y}\rho) + \nabla \cdot (Y\rho\dot{\boldsymbol{u}}) = \Psi.$$

We model the one-step reaction with the following Arrhenius law [36]:

$$\Psi = -kY\rho \exp\left(-\frac{E_A\rho}{p}\right).$$

The pressure p is obtained from the equation of state

$$p = (\gamma - 1)(\rho e - \rho Y q),$$

where the parameter q denotes the heat release due to the chemical reaction per unit mass, which determines the detonation speed uniquely [36]. In the specific case considered here, we utilize the constant volume burn model suggested by Mader [37]. This model neglects the detailed chemical depletion and, therefore, the internal detonation structure, but ensures the right propagation speed and the correct state in chemical equilibrium at all grid resolutions.

The model is intended to be applied together with the fractional step method, which numerically decouples the chemical reaction and the hydrodynamic transport. From the detonation simulation, we obtain the pressure applied as the boundary condition to the shell. The pressure time history at the notch location of one particle is shown in Fig. 1.

We now focus on the shell fracture. The material data are $E = 69$ GPa, $\rho = 2719$ kg/m^3, $\nu = 0.33$, $\sigma_0 = 275$ GPa, $\varepsilon_0^p = 0.001$, $1/n = 0.07$, and $1/m = 0.01$. The cylindrical shells are modeled with up to 280,000 nodes. At least 140,000 nodes were needed until convergence of the solution was achieved. We considered experiments with three notch lengths: 1 inch (short notch), 2 inches (long notch), and 3 inches (very long notch).

For the short notch, the crack propagated initially straight in the experiment before the crack closer to the detonation curved in an 45° angle that continued to propagate in the circumferential direction. This is predicted well in the numerical simulation (Fig. 2). Cracks propagate shortly from the crack tips and then bifurcate in the circumferential direction. Similar observations were made in the experiment. The cracks are arrested after propagating approximately 3/4 of the circumference.

For the long notch, the crack pattern was similar, except that the farther crack (from the detonation) branched into circumferential cracks that propagated the entire circumference until fracture (Fig. 3). The simulation predicts catastrophic failure and captures the basic failure pattern, i.e., formation of short cracks and crack propagation in the circumferential di-

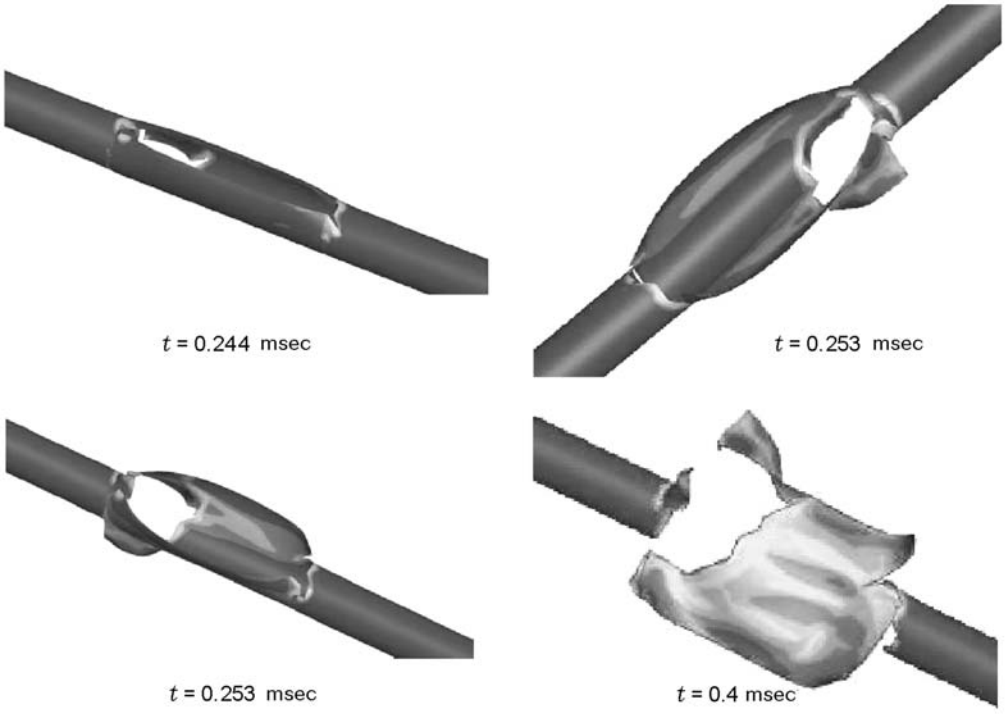

Fig. 4. Displaced configuration and effective stress of the detonation-driven fracture of a cylinder at different times (the notch length is 3 inches).

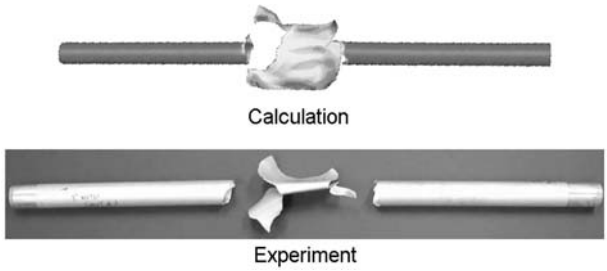

Fig. 5. Displaced configuration and effective stress of the detonation-driven fracture of a cylinder (t = 0.4 msec; the notch length is 3 inches).

rection. However, the simulation does not predict the crack curving on the side closer to the detonation. Instead, the crack branches and propagates in two directions in the circumferential direction, as opposed to only one circumferential crack observed in the experiment. The complete failure on the other side of the shell was not predicted by the simulation either. We attribute these differences to our simplified fracture model and to the fact that the fluid–structure interaction is neglected (this interaction can have significant influence on the pressure in the gas).

For the very long notch, catastrophic failure happened in the experiment. Cracks propagated straight from the notch before they branched into the circumferential direction and some minor branches. These cracks propagated over the entire circumference and led to the complete failure (on both sides) of the tube. This was also predicted in our numerical simulation (Figs. 4 and 5).

CONCLUSIONS

We predicted the failure of the tubes with short and very long notches accurately. The largest discrepancies with the experiments (we performed comparisons with the data [35]) occurred for the transition case, i.e., the tube with the long notch. We attribute these discrepancies to our simplified failure model and the fact that the fluid–surface interaction effects are neglected. For the extreme cases of the very long notch and short notches, the approximation of the pressure from a pure detonation simulation in a rigid tube seems to be adequate.

Therefore, our future research will focus on more advanced fracture models of the shell by, for example, using cohesive zone models and discrete cracks, as proposed, e. g., in [18, 38–41]. We will also develop a model of fluid–surface interaction.

REFERENCES

1. V. I. Bolobov and N. A. Podlevskikh, "Mechanism of metal ignition due to fracture," *Combust., Expl., Shock Waves*, **43**, No. 4, 405–413 (2007).
2. V. I. Bolobov, "Mechanism of self-ignition of titanium alloys in oxygen," *Combust., Expl., Shock Waves*, **38**, No. 6, 639–645 (2002).
3. S. G. Vadchenko, N. T. Balikhina, and V. L Kvanin, "Combustion of hollow cylinders," *Combust., Expl., Shock Waves*, **38**, No. 4, 425–429 (2002).
4. A. V. Gerasimov, "Protection of an explosion chamber against fracture by a detonation wave," *Combust., Expl., Shock Waves*, **33**, No. 1, 111–116 (1997).
5. Yu. I. Voitenko, "Fracture of solids by weak blasts," *Combust., Expl., Shock Waves*, **31**, No. 4, 492–499 (1995).
6. N. N. Pilyugin, "Destruction of filled polymer targets by high-velocity impact," *Combust., Expl., Shock Waves*, **44**, No. 2, 239–247 (2008).
7. T. Belytschko, Y. Y. Lu, and L. Gu, "Element-free Galerkin methods," *Int. J. Numer. Methods Eng.*, **37**, 229–256 (1994).
8. W. K. Liu, S. Jun, and Y. F. Zhang, "Reproducing kernel particle methods," *Int. J. Numer. Methods Eng.*, **20**, 1081–1106 (1995).
9. W. K. Liu, S. Hao, T. Belytschko, S. F. Li, and C. T. Chang, "Multiple scale meshfree methods for damage fracture and localization," *Comput. Mater. Sci.*, **16**, Nos. 1–4, 197–205 (1999).
10. W. K. Liu, S. Hao, T. Belytschko, S. F. Li, C. T. Chang, "Multi-scale methods," *Int. J. Numer. Meth. Eng.*, **47**, No. 7, 1343–1361 (2000).
11. S. Hao, H. S. Park, and W. K. Liu, "Moving particle finite element method," *Int. J. Numer. Meth. Eng.*, **53**, No. 8, 1937–1958 (2002).
12. S. Hao, W. K. Liu, and T. Belytschko, "Moving particle finite element method with global smoothness," *Int. J. Numer. Meth. Eng.*, **59**, No. 7, 1007–1020 (2004).
13. T. Rabczuk and T. Belytschko, "Cracking particles: a simplified meshfree method for arbitrary evolving cracks," *Int. J. Numer. Meth. Eng.*, **61**, No. 13, 2316–2343 (2004).
14. T. Rabczuk and J. Eibl, "Simulation of high velocity concrete fragmentation using SPH/MLSPH," *Int. J. Numer. Meth. Eng.*, **56**, 1421–1444 (2003).
15. S. R. Idelsohn, E. Onate, and F. Del Pin, "The particle finite element method: a powerful tool to solve incompressible flows with free surfaces and breaking waves," *Int. J. Numer. Meth. Eng.*, **61**, 964–989 (2004).
16. S. Hao, W. K. Liu, and D. Qian, "Localization-induced band and cohesive model," *Trans. ASME, J. Appl. Mech.*, **67**, No. 4. 803–812 (2000).
17. T. Rabczuk and T. Belytschko, "Adaptivity for structured meshfree particle methods in 2D and 3D," *Int. J. Numer. Meth. Eng.*, **63**, No. 11, 1559–1582 (2005).
18. T. Rabczuk, T. Belytschko, and S. P. Xiao, "Stable particle methods based on lagrangian kernels," *Comp. Meth. Appl. Mech. Eng.*, **193**, 1035–1063 (2004).
19. T. Rabczuk, P. M. A. Areias, and T. Belytschko, "A simplified meshfree method for shear bands with cohesive surfaces," *Int. J. Numer. Meth. Eng.*, **69**, No. 5, 993–1021 (2007).
20. S. Hao, W. K. Liu, P. A. Klein, and A. J. Rosakis, "Modeling and simulation of intersonic crack growth," *Int. J. Solids Struct.*, **41**, No. 7, 1773–1799 (2004).
21. S. Hao and W. K. Liu, "Moving particle finite element method with super-convergence: Nodal integration formulation and applications," *Comp. Meth. Appl. Mech. Eng.*, **195**, Nos. 44–47, 6059–6072 (2006).
22. P. Krysl and T. Belytschko, "Analysis of thin shells by the element-free galerkin method," *Int. J. Numer. Meth. Eng.*, **33**, 3057–3078 (1996).
23. T. Rabczuk, P. M. A. Areias, and T. Belytschko, "A meshfree thin shell method for non-linear dynamic fracture," *Int. J. Numer. Meth. Eng.*, **72**, No. 5, 524–548 (2007).
24. T. Rabczuk and P. Areias, "A meshfree thin shell for arbitrary evolving cracks based on an extrinsic basis," *CMES-Comp. Model. Eng. Sci.*, **16**, No. 2, 115–130 (2006).
25. B. M. Donning and W. K. Liu, "Meshless methods for shear-deformable beams and plates," *Comp. Meth. Appl. Mech. Eng.*, **152**, Nos. 1–2, 47–71 (1998).
26. W. Kanok-Nukulchai, W. Barry, K. Saran-Yasoontorn, and P. H. Bouillards, "On elimination of shear locking in the element-free Galerkin method," *Int. J. Numer. Meth. Eng.*, **52**, 705–725 (2001).
27. H. Noguchi, T. Kawashima, and T. Miyamura, "Element free analysis of shell and spatial structures," *Int. J. Numer. Meth. Eng.*, **47**, 1215–1240 (2000).
28. D. D. Wang and J. S. Chen, "A locking-free meshfree curved beam formulation with the stabilized conforming nodal integration," *Comput. Mech.*, **39**, No. 1, 83–90 (2006).
29. G. Yagawa and T. Miyamura, "3-node triangular shell element using mixed formulation and its implementation by free mesh method," *Comput. Struct.*, **83**, 2066–2076 (2005).
30. S. Li, W. Hao, and W. K. Liu, "Numerical simulations of large deformation of thin shell structures using meshfree methods," *Comput. Mech.*, **25**, 102–116 (2000).
31. M. Zhou, G. Ravichandran, and A. J. Rosakis, "Dynamically propagating shear bands in impact-loaded prenotched plates. 2. Numerical simulations," *J. Mech. Phys. Solids*, **44**, No. 6, 1007–1032 (1996).
32. D. Peirce, C. F. Shih, and A. Needleman, "A tangent modulus method for rate dependent solids." *Comput. Struct.*, **18**, 875–887 (1984).

33. T. Belytschko and Y. Y. Lu, "Element-free galerkin methods for static and dynamic fracture," *Int. J. Solids Struct.*, **32**, 2547–2570 (1995).
34. T. Belytschko, Y. Y. Lu, and L. Gu, "Crack propagation by element-free Galerkin methods." *Eng. Fract. Mech.*, **51**, No. 2, 295—315 (1995).
35. T. W. Chao, "Gaseous detonation-driven fracture of tubes," Ph. D. Thesis, California Institute of Technology (2004).
36. W. Fickett and W. C. Davis, *Detonation*, University of California Press, Berkeley (1979).
37. C. L. Mader, *Numerical Modeling of Detonations*, Univ. of California Press, Berkeley (1979).
38. T. Rabczuk and T. Belytschko, "A three dimensional large deformation meshfree method for arbitrary evolving cracks," *Comput. Meth. Appl. Mech. Eng*, **196**, 2777–2799 (2007).
39. G. Zi, T. Rabczuk, and W. Wall, "Extended meshfree methods without branch enrichment for cohesive cracks," *Comput. Mech.*, **40**, No. 2, 367–382 (2007).
40. T. Rabczuk and T. Belytschko, "Application of particle methods to static fracture of reinforced concrete structures," *Int. J. Fracture*, **137**, Nos. 1–4, 19–49 (2006).
41. T. Rabczuk and G. Zi, "A meshfree method based on the local partition of unity for cohesive cracks," *Comput. Mech.*, **39**, No. 6, 743–760 (2007).